JOURNAL OF GEOPHYSICAL RESEARCH, VOL. 111, C09015, doi:10.1029/2005JC002900, 2006

Observations of the sea surface by coherent L band radar at low grazing angles in a nearshore environment

P. Forget,[1] M. Saillard,[1] and P. Broche[1]

Received 28 January 2005; revised 15 July 2005; accepted 8 March 2006; published 13 September 2006.

[1] Coherent microwave L band signals have been collected in a Mediterranean coastal zone in horizontal transmit/horizontal receive (HH) and vertical transmit/vertical receive (VV) polarization modes at low grazing angles and under light to strong wind conditions. Doppler spectra have distinct morphologies depending on polarization mode and wind conditions. VV spectra and, only under light wind conditions, HH spectra present features that are consistent with an interaction process of Bragg type between electromagnetic waves and the sea surface, including the Doppler effects imparted by surface currents. At high wind, fast scatterers associated with greater velocities than Bragg velocity can be detected on HH spectra, depending on the direction of propagation of long waves and not on wind direction, these directions being not necessarily the same in the coastal zone considered. For a given radar range the backscattered power in VV was found to be almost constant, which suggests saturation of the wave spectrum in the short-wave range and isotropy of the short-wave spectral energy in the downwind half plane. For vertical polarization the observed variations of the relative backscattering coefficient with grazing angle are supported by the slightly rough surface scattering theory, but the HH/VV polarization ratio is much greater than predicted by this theory. The data suggest that at low grazing angles, non-Bragg scattering effects play a major role at horizontal polarization, especially in high-wind–high-wave conditions.

Citation: Forget, P., M. Saillard, and P. Broche (2006), Observations of the sea surface by coherent L band radar at low grazing angles in a nearshore environment, *J. Geophys. Res.*, *111*, C09015, doi:10.1029/2005JC002900.

1. Introduction

[2] Numerous experimental and theoretical studies have been conducted over the past decades to better understand the Doppler spectral signatures of the sea surface at microwave frequencies. These studies were and are still motivated by the development of active remote sensing instruments, particularly spaceborne (SAR, scatterometer, altimeter), and also by the use of coherent microwave radars to measure properties of short surface waves, in the centimeter-decimeter range, which are very difficult to investigate using in situ sensors.

[3] Most of these studies considered at least two polarization modes, VV (vertical transmit/vertical receive) and HH (horizontal transmit/horizontal receive). Intriguing differences between the radar signatures corresponding to these modes gradually came out from experiments both in tank and at sea. In particular, as the incidence angle increases from small to large, the dominant peak of horizontally polarized Doppler spectra is shifted toward higher frequencies than in the corresponding vertically polarized spectra. This was recently observed at X band frequencies both at sea [*Lee et al.*, 1995, 1996; *Plant*, 1997] and in tank [*Lee et al.*, 1998; *Sletten and West*, 2003], and in Ku band at sea [*Rozenberg et al.*, 1996] and in tank [*Plant et al.*, 1999; *Rozenberg et al.*, 1999]. The separation of HH and VV spectral peaks was interpreted as the manifestation of bound waves and/or non-Bragg scattering mechanisms occurring, for instance, in wave breaking conditions. The paper by *Lee et al.* [1999] provides a stimulating discussion of these effects.

[4] Advanced electromagnetic computer codes have been developed, in recent years, to model the coherent radar response of linear and nonlinear water surfaces [*Toporkov and Brown*, 2000; *Johnson et al.*, 2001; *Toporkov and Brown*, 2002; *Lamont-Smith*, 2003; *Hayslip et al.*, 2003]. These simulations as well as more classical approaches using the composite model [*Plant*, 1997] tend to confirm the contribution of water profile nonlinearities to explain the differences between HH and VV Doppler spectra.

[5] Other issues related to radar sensing of the sea at low grazing angle concern the sensitivity of the scattered power to wind conditions, the power polarization ratio HH/VV, which is often higher than expected from theory, and the variation with distance or incidence angle of radar backscattered power, which is a recurrent subject of controversy [e.g., *Barrick*, 1998].

[6] This study presents and interprets a unique set of dual-polarized data in L band collected by a ground-based radar. Owing to the size and weight of the antennas, which reduced the flexibility of their installation for sea observa-

[1]Laboratoire de Sondages Electromagnétiques de l'Environnement Terrestre, CNRS, Université du Sud Toulon-Var, La Garde, France.

0148-0227/06/2005JC002900$09.00

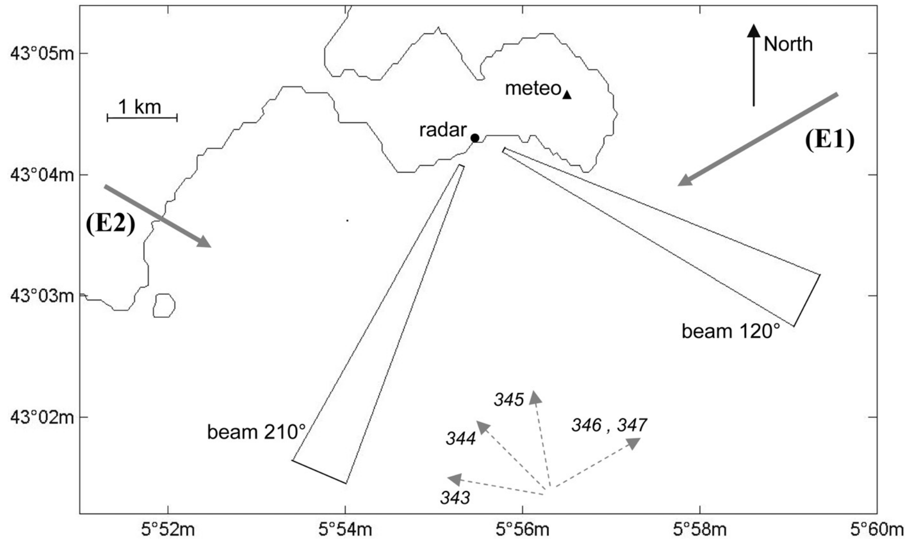

Figure 1. Geography of the experimental field. Directions refer to geographical north. The radar beams are schematized by trapezes whose dimensions correspond to the range of radial distances and to the 3 dB beam width of the antennas. Shaded arrows are the directions of the wind for wind episodes (E1) (right) and (E2) (left). Dashed arrows are the swell directions for the Julian days indicated.

tion, the radar was constrained to operate at low grazing angles (<12°).

[7] The experiment is described in section 2. Results for the morphology of Doppler spectra are given in section 3. The Doppler shifts measured for vertically and horizontally polarized modes are presented in section 4. Energy considerations relative to the variation of VV backscattered power with wind and grazing angle, and the values of the polarization ratio are given in section 5.

2. Experiment

[8] The experiment was conducted during 9 days in December 2003, near Toulon, south of France (Figure 1).

2.1. Radar Deployment

[9] We used a coherent pulsed L band radar designed and manufactured by Degréane Horizon company (Cuers, France). The radar, which is primarily dedicated to wind speed and turbulence measurements in the troposphere, can work with several transmitting/receiving (T/X) antennas [*Bénech et al.*, 2000]. Each antenna consists of an array of 8 × 8 25 dBi dipoles forming 8 parallel tubes mounted over a metallic panel of size 2 m (along the tube axis) × 1.67 m. For atmospheric applications, the radar typically uses five antennas pointing vertically or obliquely. The theoretical characteristics of the antenna pattern are given in Table 1.

[10] The radar system was mounted on a concrete platform at the top of a sheer cliff (altitude 91 m). The layout of the antennas was modified to allow sea surface observation (Figure 2). The antennas were fixed on a metallic structure consisting of two perpendicular arms welded together and lying on the platform. Two antennas were disposed on each arm of the structure. They differed by the orientation of the dipole axis, horizontal and vertical, corresponding to HH and VV T/X operating modes, respectively. The azimuths of observation of the two pairs of antennas, at 120° and 210° from geographic north, are shown in Figure 1. The four antennas will be termed 120HH, 120VV, 210VV and 210HH.

[11] The plane of the antennas was slightly tilted from vertical (5°) to allow the main beam of each antenna to point at the sea surface at a distance of 1055 m. This way, given the antenna characteristics, the sampled radar sea cells (Table 2) were all located within the main beam. Assuming that the azimuthal width of the radar cells only depends on the horizontal width of the main beam, its value varies approximately from 80 m (first cell) to 1000 m (last cell). The range resolution has a constant value of 75 m.

[12] Figure 3 shows the theoretical variations with range of the weighting factor affecting the backscattered signal power. The weighting factor was computed from the radiation pattern of the antennas. The grazing angle, α, corresponding to the radar cells is plotted on Figure 3; α varies from 10.7° at the nearest range to 0.9° at the largest.

2.2. Radar Measurements

[13] A cycle of radar measurements consisted of four data sets which were consecutively acquired by antennas 120HH to 210HH, respectively (Table 2). The typical dwell time of a data set was 30 s resulting in a cycle time of about 2 min. A radar cycle then provides observations of the sea at HH and VV polarizations within a time interval which is small as compared to the typical sea state and wind stationarity timescales.

Table 1. Main Characteristics of the Antennas[a]

	E Plane	H Plane
Beam width, deg	10.0	8.4
First zeros, deg	±11.6	±9.5
First sidelobe, deg	±15.0	±13.0
First sidelobe rejection, dB	14.0	17.0

[a]Directions of the first zeros of the antenna pattern and of the first sidelobe refer to the azimuth of the maximum of the main beam.

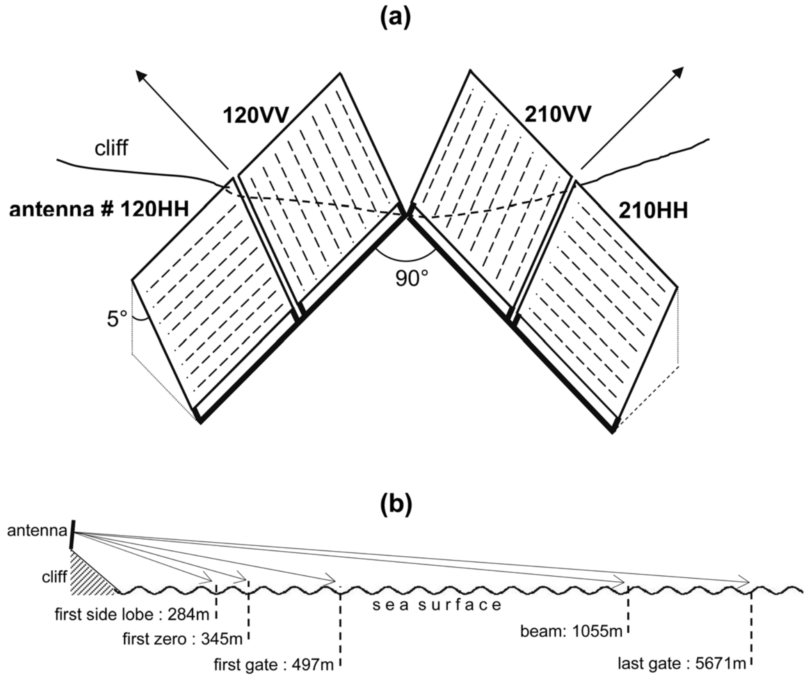

Figure 2. Radar antennas. (a) Top slant view of the antennas. The metallic structure supporting the antennas is shown in bold. Dashed lines indicate dipole arrays. (b) Schematic view of the antenna pattern in a vertical plane.

[14] For a given interpulse period, IPP, and a given number of spectral points, an important data processing parameter is the number of coherent integrations, NCI, which governs the spectral bandwidth, Δf, and the spectral resolution, δf. The lessons learned from two preliminary short experiments [*Forget et al.*, 2003a, 2003b] suggested NCI values of 150 (VV) and 60 (HH). Because the radar was generally operated automatically, with a limited number of interrupts, NCI was not always optimized regarding the spectral bandwidth which turned out to vary with wind and wave conditions. We used NCI = 40 (Δf = 250 Hz, δf = 2.0 Hz), 80 (125 Hz, 1.0 Hz), 100 (100 Hz, 0.78 Hz) or 150 (66.7 Hz, 0.52 Hz) for horizontal polarization, and NCI = 100 or 150 for vertical polarization.

[15] The theoretical number of degrees of freedom of Doppler spectra, D, was equal to 20. Without losing information on the content of the spectra (except for some rapidly varying events), we could increase D from 20 to 30 to 35 by incoherent summation of the spectra over 20 min. This duration corresponds to the typical stationarity time-scale of ocean waves; for example, it is considered for the computation of wave spectra from the time series collected by a wave rider buoy.

[16] The radar was not calibrated and thus power or power density values differ from absolute values by an unknown multiplicative term. However, this term can be expected to be only slightly dependent on the considered antenna. Indeed, the antenna patterns were quite similar (Table 1) and the electrical ground of the antennas was homogeneous. Furthermore, the transmitting and receiving chains were switched between the antennas using coaxial cables of the same length. We verified that the noise levels for the four antennas generally differed by less than 1 dB. As the noise power is essentially determined by the losses in the antenna distribution network, this suggests only little imbalance between the receiving chains. This can be extended to the transmitting chains since the system is monostatic.

2.3. Environmental Conditions

[17] Hourly wind speeds and directions were measured near the radar by a meteorological station of the French meteorological office Meteofrance. Three main wind regimes were encountered (Figure 4): an east-north-east wind episode (Julian days 343–344) with velocities, W, up to 13 m s^{-1}; then a period of low winds ($W < 5$ m s^{-1}) with varying velocities and directions (days 345–347); and a west-north-west wind period (days 347–350) with velocities up to 21 m s^{-1}. The first and last periods will be termed (E1) and (E2) in the following and will be associated with "high winds" (>5 m s^{-1}). The wind directions corresponding to (E1) and (E2) are shown in Figure 1.

[18] An omnidirectional wave rider buoy was deployed 1 km to the southwest of the radar beam pointing to 210°. Water depth was 50 m. The buoy provided wave data sets of

Table 2. Main Radar and Data Processing Characteristics

Characteristic	Value
Frequency	1.238 GHz
Radar wavelength	0.24 m
Peak power	4000 W
Interpulse period	100 μs
Pulse width–range resolution	0.5 μs–75 m
Number of coherent integrations	varying (40 to 150)
Number of incoherent integrations	20
Range sampling (middle of radar cells)	496–5671 m
Range gating	75 m
Number of FFT points	128

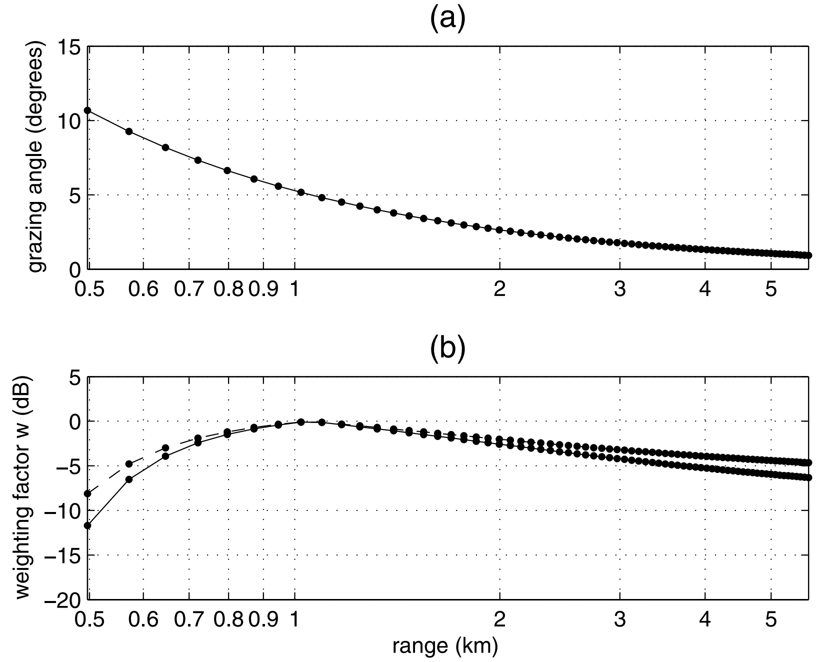

Figure 3. Variation with range of the (a) grazing incidence angle and (b) power weighting factor due to the antenna pattern in a vertical plane. Top (bottom) curve is VV (HH) polarization.

20 min every 30 min with a sampling frequency of 2.56 Hz. For logistical reasons, the buoy could not be moored along or between the radar beams as was initially planned. Hence the collected wave data cannot always apply to the radar cells, in particular during the west-north-west wind period, which corresponds to short fetch conditions. Significant wave height (H_S) values up to 1.5 m were recorded during the first wind episode and in the interval 0.4–1 m for the other periods. The wave spectra peaks in low wind conditions were associated with incoming offshore swells.

[19] We collected five days of observations at sea. These were performed on a small boat sailing inside the radar beams. The observations were made at 1, 2, 3 and 4 km from the radar, twice a day along each radar beam, and consisted of visual estimates of wave direction and sea roughness and of surface current measurements. The current vectors were obtained from the trajectories of a small drifter tracked by GPS. The drifter was released during 7 min at each station. The integration depth under the sea surface of current measurements was estimated to be less than 5 cm. Swell was observed at sea with characteristics given in Table 3 and directions shown in Figure 1.

3. Morphology of Doppler Radar Spectra

[20] Figure 5 shows examples of spectra measured by the four antennas, typical of the three main wind conditions. For convenience, Doppler frequencies, f_D, were converted into Doppler velocities $V_D = \lambda f_d/2 \cos \alpha$, with λ the radar wavelength. V_D is the component in the plane of incidence of the velocity of horizontally moving scatterers, or whatever horizontal motion, causing f_D.

3.1. Morphology for Low-Wind Conditions

[21] The dominant features of Doppler spectra (Figures 5a and 5b) are in this case similar to the general features which have been often described in the literature and which apply to a broad interval of the electromagnetic spectrum: HF band [*Barrick*, 1972; *Forget et al.*, 1981], VHF band [*Broche et al.*, 1987], L and Ku bands [*Plant and Keller*,

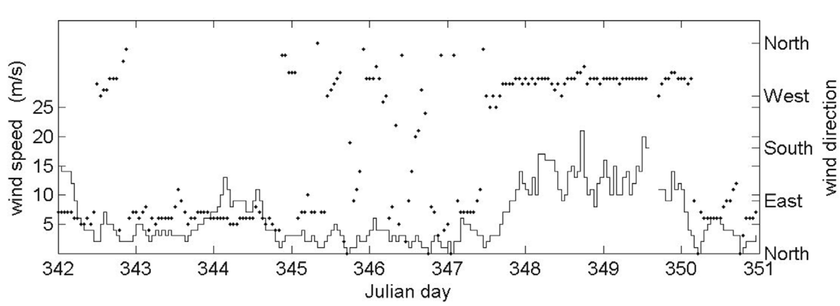

Figure 4. Wind intensity and direction recorded by the meteorological station (see Figure 1).

Table 3. Swell Characteristics From Observations at Sea and From Wave Spectra Measurements: Significant Wave Height, H_S, Peak Frequency, F_p, and Direction of Propagation[a]

Julian Day	H_S, m	F_p, Hz	Direction
343	0.80	0.16	west
344	1.54	0.15	north-west
345	0.64	0.17	north-north-west
346	0.50	0.18	north-east
347	0.38	0.17	east-north-east

[a]Values are averaged over 4 hours.

1990] and X band [*Valenzuela*, 1974]. First, the energy is concentrated in the vicinity of the Bragg velocities, $\pm V_B$, where V_B is given by

$$V_B = \left(\frac{g\lambda}{4\pi\cos\alpha}\right)^{1/2}, \quad (1)$$

with g the gravity acceleration. For present values of α, V_B is close to 0.43 m s^{-1}. Furthermore, the left-right asymmetry of the radar spectra with respect to the null Doppler velocity is mainly governed by the wind direction.

[22] For illustration, VV Doppler spectra of Figures 5a and 5b were qualitatively reproduced using the classical model of first- and second-order Doppler spectrum established by *Barrick* [1972] (Figures 6a and 6b). Wind speed was 2 m s^{-1} and the wave spectrum was modeled by the Pierson-Moskowitz spectrum with a distribution function proportional to $\cos^3(\theta-\theta_W)/2$. Here θ and θ_W are the wave and wind directions relative to the radar line-of-sight direction, respectively. An east-north-east wind direction was assumed. However, results of Barrick's model are only indicative since its validity requires $m = 2\pi\sigma/\lambda < 0.3$ with σ the RMS of the sea surface elevation [*Lipa and Barrick*, 1986]. This condition was hardly satisfied here ($m = 0.55$). This could explain why the experimental spectra are wider than the computed spectra (a similar difference was noticed in VHF radar spectra [*Broche et al.*, 1987]) and why the portion of the spectra lying between the two peaks is more filled up than in the theoretical spectra. It should be noticed that the frequency sampling in Figure 6 is the same as the experimental one. Then, as for the experimental Doppler spectra, the Bragg lines are not well resolved and the two "peaks" observed in the vicinity of the Bragg velocities include, in fact, first- and second-order contributions. In those cases of low wind, spectra in HH and VV present the

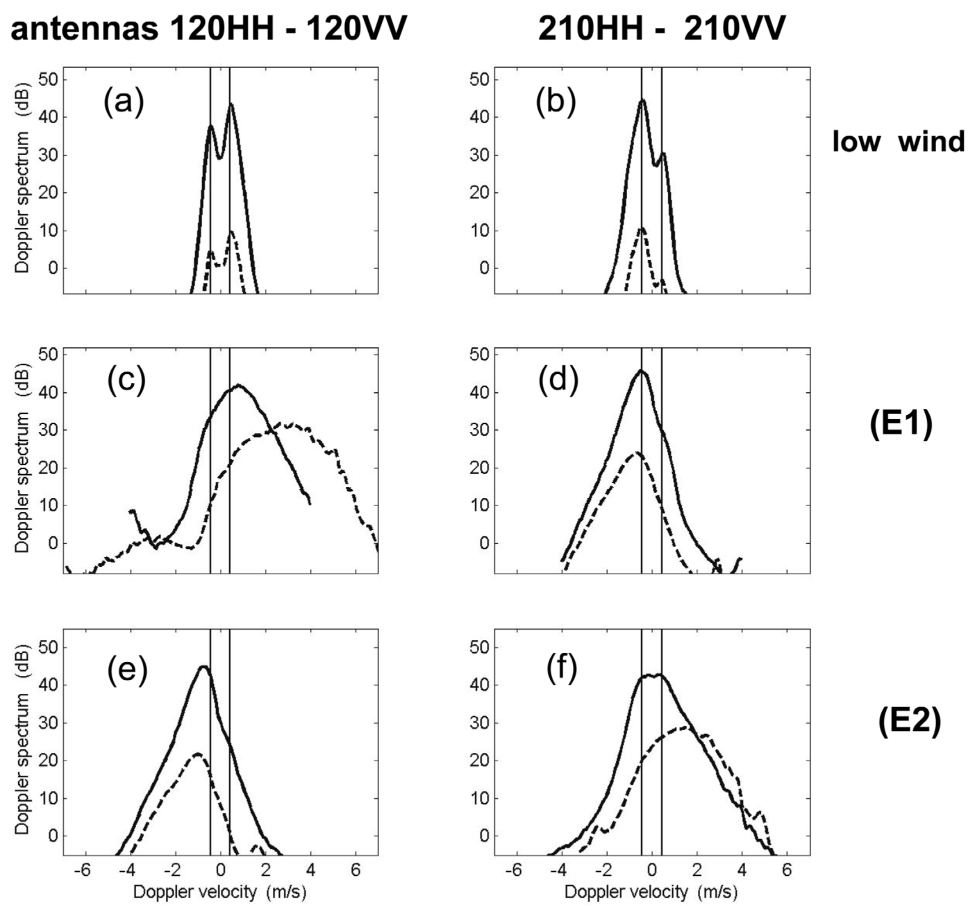

Figure 5. Examples of Doppler spectra (a and b) in VV (solid line) and HH (dashed line) for low winds and wind episodes (c and d) (E1) and (e and f) (E2) at radar cell number 14 (radial distance 1471 m, $\alpha = 3.6°$). Antennas are (left) 120HH and 120VV and (right) 210HH and 210VV. Vertical lines refer to the positions of theoretical Bragg velocities without current.

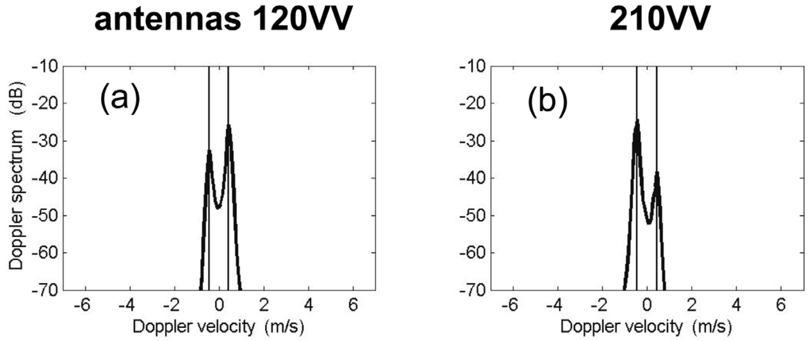

Figure 6. Theoretical Doppler spectra in (a) 120VV and (b) 210VV polarization using *Barrick*'s [1972] model and corresponding to the experimental spectra of Figures 5a and 5b.

same aspect with smaller values in HH than in VV (see section 5.3).

3.2. Morphology for High-Wind Conditions

[23] For wind events (E1) and (E2) (Figures 5c and 5d and 5e and 5f, respectively), vertically polarized spectra generally show two maxima or "shoulders" in the vicinity of Bragg velocities. However, spectra are much wider than at low wind with a spectral bandwidth depending on the considered radar line of sight.

[24] A characteristic of VV Doppler spectra is the clear dependence on wind direction of the left-right asymmetry of these spectra in their central part (typically in the velocity interval $[-2V_B, +2V_B]$). Let us define the central asymmetry factor, A_c, as the ratio of the energies of the peaks at positive and negative velocities. The energy of a peak was computed by integrating the spectrum over, typically, 4 Doppler velocity intervals in the vicinity of the peak position. As only one peak was generally present, at velocity V_{max}, the other velocity interval was defined in the vicinity of $V_{max} - 2\ \mathrm{sign}(V_{max})\ V_B$. Figure 7 shows the diagram of A_c values measured on antennas 210VV, A_{c210}, and 120VV, A_{c120}, for wind episodes (E1) and (E2). The data points form two distinct clouds centered on mean values $A_{c210} = -7.5$ dB, $A_{c120} = 3.6$ dB (E1) and $A_{c210} = 2.8$ dB, $A_{c120} = -14.0$ dB (E2). Rearranging these values versus the absolute value of the wind direction angle relative to the radar axis, θ_r, we obtain: $A_c = -14, -7.5, 2.8, 3.6$ dB for $\theta_r = 0°, 30°, 90°, 120°$, respectively. Thus A_c monotonically increases from downwind ($\theta_r = 0°$) to upwind look direction and changes of sign near crosswind ($\theta_r = 90°$). These results show that the central part of Doppler spectra for vertical polarization depends on wind direction as in the low-wind case. This suggests that the central part of VV spectra is dominated by radar wave-ocean wave interaction processes of Bragg type.

[25] Doppler spectra for HH polarization can be very different from those in VV polarization (Figures 5c-5f). The main differences concern the spectral shape of these spectra, which is often characterized by a bell-shaped peak whose width is larger than the width of the corresponding peak in VV polarization mode; and the position of the maximum of the peak, which can be at greater Doppler velocities than in the VV case. These differences depend on the radar look direction; for example, the spectrum in HH is narrower with a spectral peak closer to V_B for antenna 210HH than for 120HH in Figures 5d and 5c and vice versa in Figures 5e and 5f. Following the terminology of *Lee et al.* [1995], Doppler peaks can be "fast" or "slow" depending on the shift of the maximum from the Bragg velocity. Large shifts are associated with "fast scatterers." The occurrence of fast scatterers corresponds to a departure of the electromagnetic interaction process from the Bragg regime and/or to non-linearities of the hydrodynamic processes. The new result obtained here is that, for the same wind conditions, the spectral peak in HH can be fast or slow depending on the radar look direction. The analysis of Doppler velocities of the spectral peak and interpretation are reported in section 4.

[26] The last point seems important. Outside the central part of vertically polarized radar spectra, we sometimes noticed an asymmetry of energy that was not correlated with wind direction. For illustration, let us define the lateral asymmetry factor, A_l, as the ratio of the energies in the

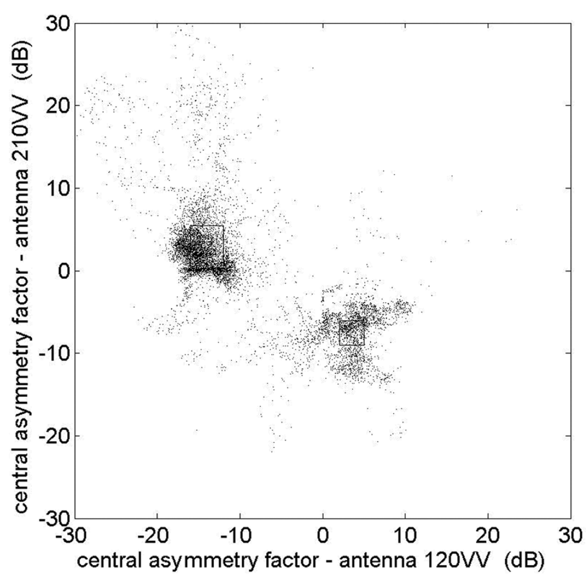

Figure 7. Comparison of the central asymmetry factor of radar spectra, A_c, for azimuths 210VV and 120VV and for wind episodes (E1) and (E2). Rectangles are centered on the mean values of data points corresponding to (E1) (right) and (E2) (left), respectively. The horizontal and vertical length of the rectangles are equal to the standard deviations of A_c values.

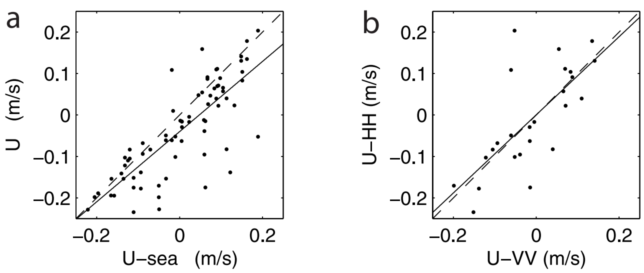

Figure 8. Comparison of radar and in situ measurements of surface currents, U and U_{sea}, respectively. (a) All data. Bold line is the regression line; dashed line is the fit. (b) Comparison of radar estimates for polarizations HH and VV, U_{HH} and U_{VV}, respectively.

intervals $[2V_B, V_N]$ and $[-V_N, -2V_B]$ with $\pm V_N$ the limits of the Doppler velocity interval of the spectrum. On Figure 5f A_c is close to 1, which is typical of a crosswind behavior, whereas A_l is much greater. In fact, such lateral asymmetry of VV spectra was always associated with fast peaks in the corresponding HH spectra as on Figure 5f. In Figure 5c, where the central asymmetry of the spectrum in VV is high because of quasi-upwind conditions, the fast scatterers observed on the corresponding HH spectrum contribute here as well to enrich the radar backscatter energy at high Doppler velocities. This is less clear in Figures 5d and 5e because HH spectra are only little fast in this example. These observations suggest that fast scatterers are detected in both vertically and horizontally polarized spectra, but with a less important relative energetic contribution in VV.

4. Doppler Velocity of the Spectral Maximum

[27] This parameter, V_m, was determined using a centroid method applied in the vicinity of the maximum of each Doppler spectrum. The resulting current resolution was smaller than, e.g., 0.06 m s^{-1} for NCI = 150.

4.1. Comparison With in Situ Current Measurements

[28] As radar echoes are due to scatterers linked to the sea surface, a surface current manifests itself as a Doppler shift of the radar signature of these scatterers. In HF/VHF, surface currents are measured from the spectral position of the first-order (Bragg) lines, which are associated with Bragg waves [e.g., *Stewart and Joy*, 1974; *Barrick et al.*, 1977; *Forget et al.*, 1990]. In L band, Bragg lines are discernible from the higher-order continuum only in low-wind conditions [*Wright*, 1978; *Plant and Keller*, 1990]. These conditions were met during the experiments at sea (wind velocity lower than 4 m s^{-1}) for which surface current measurements were collected. The current component along the radar beam axis, U, positive by convention for a current receding from the radar, is given by

$$U = sV_B - V_m, \qquad (2)$$

with $s = \mathrm{sign}(V_m)$. Note that the conventions of sign for U and V_D are different. Equation (2) is commonly used for current measurements by HF/VHF radars. However, we recall that the actual spectral sampling was too coarse to isolate the Bragg lines from the surrounding continuum. V_m is thus only an estimate of the Bragg velocity. Figure 8 compares U estimates for both polarizations with in situ current measurement values, U_{sea}, and compares HH and VV estimates, U_{HH} and U_{VV}, respectively. The agreement between radar and measured current values is quite good for the (small) range of U_{sea} values available (correlation coefficient ρ = 0.80, regression slope p = 0.85, offset off = −0.0 m s^{-1}). The agreement between U_{HH} and U_{VV} values is also significant (ρ = 0.72, p = 0.94, off = 0.0 m s^{-1}). These results indicate that, at least at low wind, the Bragg peaks of radar spectra for vertical and horizontal polarizations are shifted by surface currents in a similar way than in HF/VHF.

4.2. General Properties of Spectral Doppler Shifts

[29] V_m was computed for the whole data set. V_m was generally positive for downwind radar look directions (θ_r < 80°) and negative for upwind look directions (θ_r > 100°) (Table 4). This is well verified if we consider only the two well established wind episodes (E1) and (E2), which correspond to 53% of the data set. This is less verified, particularly in crosswind conditions and in HH polarization mode, if we include low-wind episodes. However, the statistics in this case are definitely biased because at low wind, the wind direction at sea can significantly differ from the values measured by the met station because of specific coastal meteorology effects such as sea breezes, orographic effects, etc.

[30] The values of U are displayed in Figure 9. White bands correspond to signal interrupts and white pixels to values that were rejected because of low signal-to-noise ratio. Here U, which was obtained using (2), has not necessarily the meaning of a surface current velocity. It only represents the difference between the observed shift

Table 4. Position of the Spectral Maximum at Positive and Negative Doppler Frequency[a]

	Upwind			Downwind		
Polarization	Positive	Negative	*Nb*	Positive	Negative	Nb
			All Data			
VV	7.7	92.3	25781	67.5	32.5	15032
HH	12.5	87.5	14784	43.9	56.1	5680
			Data for (E1) and (E2) Wind Episodes			
VV	4.4	95.6	13370	88.5	11.5	6930
HH	11.8	88.2	10363	82.1	17.9	3005

[a]Values are given in percentage of the number of cases, Nb.

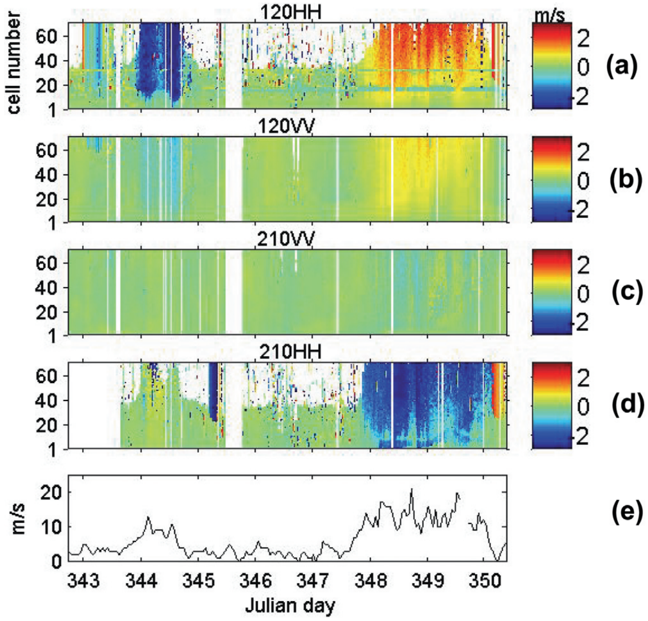

Figure 9. Variations with time and radar cell number of the Doppler velocity relative to the Bragg wave velocity, U, for antennas (a) 120HH, (b) 120VV, (c) 210VV, and (d) 210HH and the (e) wind speed record.

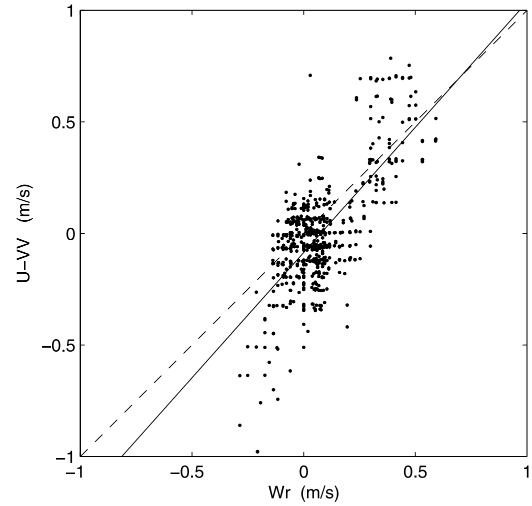

Figure 10. Comparison of U_{VV}, the difference between the peak position and the Bragg velocity for vertical polarization, for radar cells number 25 and the values of the component along the radar beams, W_r, of the wind-induced drift predicted by the model of *Madsen* [1977]. Thin line is the regression line; dashed line is the ideal fit line.

and the Bragg wave velocity, this difference resulting from all hydrodynamic effects, including currents. From histogram analysis and after rejecting spurious values, the range of U_{VV} variations was [−0.7, 0.8] m s^{-1} (antenna 120VV) and [−0.4, 0.2] m s^{-1} (antenna 210VV) and, for U_{HH}, [−4.0, 1.4] m s^{-1} (antenna 120HH) and [−2.2, 0.5] m s^{-1} (antenna 210HH). The blue band that can be observed on antenna 210HH between days 345.2 and 345.3 corresponds to spurious values (radio interference).

[31] The magnitude of U_{VV} is consistent with surface current values. For example, we considered a coarse, but popular, model of wind-induced drift stating that the surface current represents 3% of the wind speed and is orientated at 10° to the right of the wind direction [*Madsen*, 1977]. Figure 10 compares U_{VV} and W_r, the component of that drift along line-of-sight directions of the radar. The agreement is quite good ($\rho = 0.72$, $p = 1.12$, $off = -0.1$ m s^{-1}) despite some scatter (standard deviation sd = 0.2 m s^{-1}). We attribute this scatter mainly to uncertainties concerning the value of wind parameters at sea, especially at low winds. A possible contribution of the wind drift to the shift of the Doppler peak in microwaves was also reported by *Plant and Keller* [1990] and *Poulter et al.* [1994].

[32] Processes are more complex in HH polarization (Figure 11). Similar conclusions as for the VV polarization can be drawn at low winds and for antenna 210HH during the wind event (E1) ($\theta_r = 30°$). However, high approaching velocities were observed on antennas 120HH and 210HH during events (E1) ($\theta_r = 120°$) and (E2) ($\theta_r = 90°$) respectively, and high receding velocities on antenna 120HH during (E2) ($\theta_r = 0°$). These results demonstrate that, at high-wind velocities and for various wind directions, the interpretation of the Doppler shift of the spectral peak for HH polarization in terms of wind-induced currents is not sufficient. Moreover, focusing on (E1) and (E2) wind periods and except for the data corresponding to antenna 120HH, the intensity of U_{HH}, $|U_{HH}|$, generally increases with range (Figure 9).

4.3. Interpretation of Doppler Shifts at High-Wind Cases in HH

[33] We investigated the hypothesis that scatterers in those conditions are more or less linked to the dominant waves through both hydrodynamic (breaking waves, bound

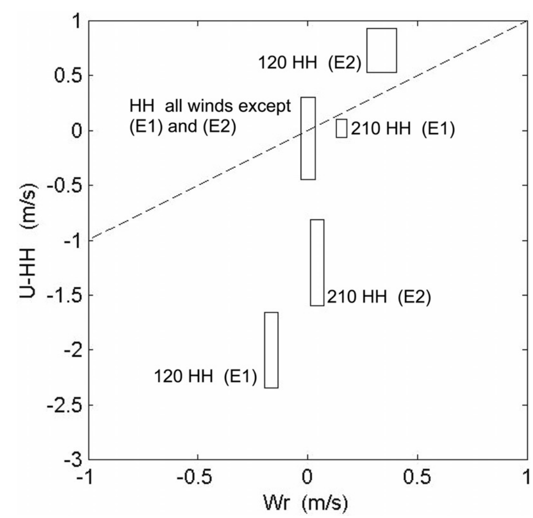

Figure 11. Same as Figure 10 for U_{HH}. The rectangles are centered on the mean values of W_r and U_{HH} for different groups of data points. (E1) and (E2) refer to the east-north-east and north-north-east well-established wind episodes, respectively. Rectangles width and height are equal to the standard deviations of W_r and U_{HH}, respectively. Dashed line is ideal fit line.

waves) and electromagnetic (shadowing effects, enhancement of surface electric currents on the wave crests) processes [e.g., *Duncan et al.*, 1974; *Ebuchi et al.*, 1992; *Rozenberg et al.*, 1996; *Lee et al.*, 1998; *Hayslip et al.*, 2003]. Specifically, we investigated that V_m, the radial component of the fast scatterers velocity, was more dependent on the dominant wave direction than on the wind direction (proportional to W_r). Since the study area was close to the coastline and since the coastline was far from being regular, it is likely that wind and dominant wave directions did not coincide. It should be noticed that, in coastal environment, a potential cause of such a difference can arise from bathymetry through refraction and diffraction effects. However, water depth was generally greater than 50 m in the area sensed by the radar (Figure 3) and then the influence of bathymetry was probably not important except near the coastline.

[34] We implemented the parametric wave model of the Great Lake Environmental Research Laboratory (GLERL, Michigan) developed in the 1980s and used, in particular, for operational wave prediction in Great Lakes of North America [*Schwab et al.*, 1984; *Liu et al.*, 1984, 2002]. The model is based on the temporal wave momentum equations in deep water with the wind as forcing term. The model is parametric in the sense that the directional wave spectrum is reduced to M, the total wave momentum, σ^2, the total wave variance, and θ_0, the mean angle of propagation, and that it assumes empirical relationships between σ^2, M and f_p (the frequency of dominant waves), and between σ^2 and f_p. These relationships are derived from the well-known JONSWAP spectral wave model. Furthermore, the wind input itself is parameterized according to M. A. Donelan (A simple wave numerical model for wave and wind stress prediction, unpublished manuscript, 1977). In order to take into account possibly large fetch effects, our computing domain was extended 220 km westward and eastward and 80 km southward. The spatial resolution was 500 m.

[35] Two wind fields were considered, corresponding to (E1) and (E2) events, but in a very simplified manner: wind was assumed homogeneous and stationary over more than 10 hours. Wind velocity was 10 m s^{-1}, which is a typical value for the two wind episodes. Obviously, simulated wave directions dramatically differ from wind directions (Figure 12). This can be explained by the influence of the complicated geometry of the coast line: presence of peninsulas 20 km to the east and a few kilometers to the west and of an island 20 km to the east, etc. Some of these wave directions were visually observed from the radar station. Although the model was not validated and thus cannot be fully used for radar interpretation, the results obtained bring coherence to the radar results of Figure 11 for wind periods (E1) and (E2). During (E1), the radar look direction for the beam axis orientated to 120° was up wave, that oriented to 210° varied with distance from cross wave to slightly down wave. During episode (E2), the first radar look direction varied from cross wave to slightly down wave offshore and the second was nearly up wave. Then, the values of U_{HH} in Figure 11 are globally consistent with a surface motion in the same direction as the dominant waves rather than in the wind direction, suggesting that U_{HH} does not represent a surface current but some fraction of the component of the dominant wave velocity along the radar look direction.

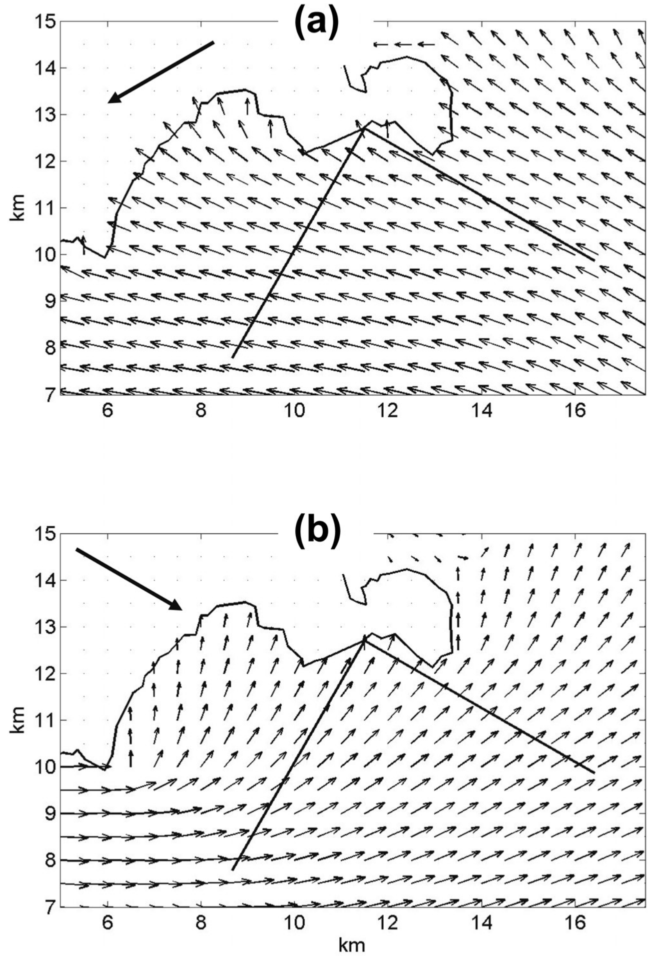

Figure 12. Mean wave directions computed by the wave model for homogeneous and stationary 10 m s^{-1} wind blowing in the directions indicated by bold arrows: (a) east-north-east-east wind (event (E1)) and (b) west-north-west wind (event (E2)). The segments draw the radar beam axis.

However, in up wave conditions, the values of $|U_{HH}|$ are only a small fraction (1/4 to 1/10) of the speed of dominant waves. This demonstrates that the scatterers responsible for the fast peaks of HH Doppler spectra are not only waves bound to the crests and advected at their velocity as suggested, mainly, by experiments in tanks [*Duncan et al.*, 1974; *Ebuchi et al.*, 1992, 1993; *Lee et al.*, 1995; *Rozenberg et al.*, 1999].

[36] Adopting the above interpretation, the increase of $|U_{HH}|$ with distance from a low value at short ranges, which is pointed out in the last section, can be explained in terms of wave direction for wind period (E1), antenna 210HH and wind period (E2), antenna 120HH. In these cases, the radar light-of-sight direction gradually turns from cross wave to down wave, involving an increase of the scatterers velocities. The case (E1) - antenna 120HH experiences a rather sharp transition from low to high values of $|U_{HH}|$ as the distance from the radar increases. This transition occurs at a distance smaller than 2 km, in a region where bathymetric effects cannot be neglected (proximity of a cape). There diffraction/refraction effects deviate the direction of the

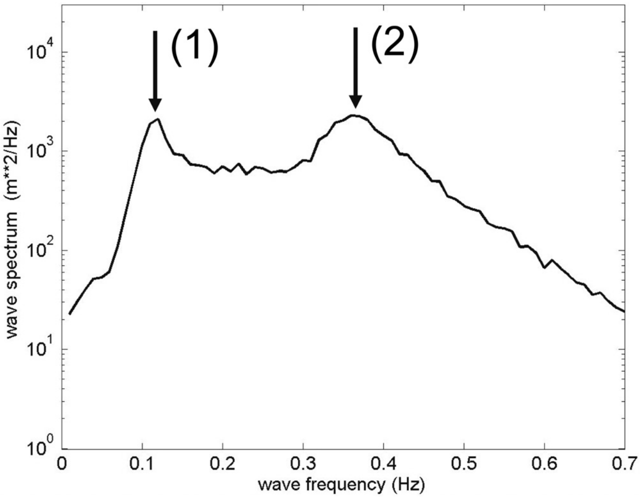

Figure 13. An example of experimental wave spectrum for a 12 m s^{-1} west-north-west wind. Peak frequencies of the two-wave systems 1 and 2 are 0.119 and 0.360 Hz; significant wave heights are 0.55 and 0.65 m.

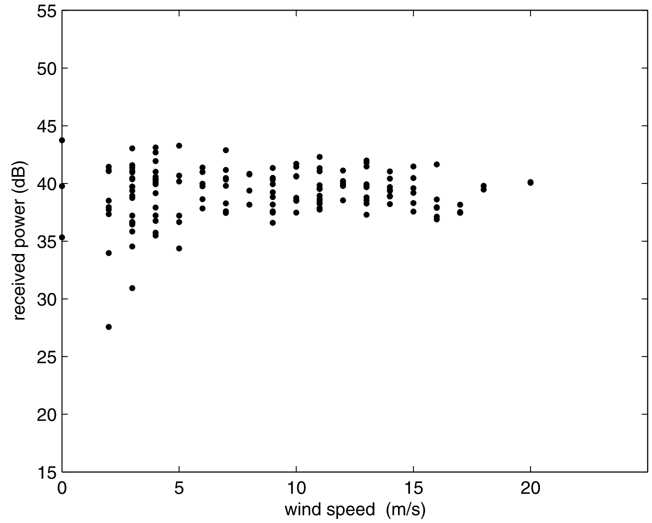

Figure 14. Variation of the received power in VV with wind speed for radar cells 18.

incoming long waves normally to the radar axis. The case (E2) - antenna 210HH is difficult to analyze because of the very complex wave conditions near the shore: the long waves coming from offshore are mixed with the short waves generated by the wind, propagating perpendicularly to the radar axis and leading to double-peak wave spectra (Figure 13). Theses waves correspond to short fetches (3–4 km) and are not resolved by the wave model which assumes a single-peak spectrum.

[37] Finally, the swell events observed and measured at sea (Table 3), corresponding to various wave/radar axis directions, were not associated with fast signals in Doppler spectra in HH polarization, excepted in the second event, which took place at the beginning of wind episode (E1). These swells were of small amplitude (H_S < 0.80 m) suggesting that the fast scatterer phenomenon in HH occurs when long waves have some specific properties, e.g., of steepness, shape and roughness, that could not be clearly specified from our data.

5. Energy Considerations

5.1. Variation of the Vertically Polarized Backscattered Power With Wind

[38] The backscattered power in VV, E_{VV}, is defined as the sum of the energies contained in the vicinity of the peaks at positive and negative velocities (see section 3.2). This was done to avoid spurious measurements in case of parasitic or undesired Doppler echoes outside the Bragg peaks. Figure 14 shows the variations of E_{VV} with wind speed and direction for the radar cells 18 (radial distance from the radar: 1771 m). Both antennas 120VV and 210VV were considered. These variations are typical of what was generally observed for the other range cells. Table 5 gives the corresponding statistics for intervals of wind speed and direction relative to the radar beam axis. The intervals were set large enough to compensate for the uncertainty concerning the exact values of offshore wind parameters. E_{VV} was found almost independent of wind conditions for $W > 5$ m s^{-1}. Low values can be found at low winds but the statistics are only slightly affected by these cases. We conclude that once W reaches some threshold value, lower than 5 m s^{-1}, the backscattering coefficient in VV (i.e., the average backscatter cross section per unit area of the sea surface), σ^0_{VV}, which is, for a given distance, proportional to the backscattered power, does not significantly vary with wind speed and direction, at least for the present crosswind to downwind conditions. In the frame of the Bragg scattering mechanism, this means that the spectral energy in the saturation range of the wave spectrum (corresponding to decimeter waves here) is hardly dependent on wind characteristics.

[39] Furthermore, we found that the sensitivity of Doppler spectra to wind direction, as exhibited in Figure 7, affected only the portion of the spectra of lowest energy, at positive or negative velocities. Within the frame of the Bragg scattering mechanism, this is consistent with an angular distribution of Bragg wave energy which is almost isotropic for wave directions extending from −90° to 90° with respect to wind direction.

[40] Similar observations were reported by *Banner et al.* [1989] who studied the wave number spectrum of short gravity waves in the wavelength range 0.2–1.6 m. Some remote sensing studies in L band lead also to similar conclusions [*Guinard et al.*, 1971; *Thompson et al.*, 1983]. The insensitivity of short-wave energy to wind speed

Table 5. Mean Values and Standard Deviation of E_{VV}, the Relative Backscattered Energy, for Radar Cells 18 and for Intervals of Wind Speed and Direction Relative to Radar Axis (Width 20°)[a]

	Wind Speed		
θ_r, deg	5 m s^{-1}	10 m s^{-1}	15 m s^{-1}
0	38.4 (2.0)	39.0 (0.9)	38.5 (1.0)
30	39.9 (2.2)	40.2 (1.6)	–
90	41.6 (1.0)	40.4 (1.1)	39.7 (1.6)
120	37.8 (2.5)	38.1 (0.9)	–

[a]Minimum number of data values considered: three. Standard deviation is given within parentheses; E_{VV} is given in dB.

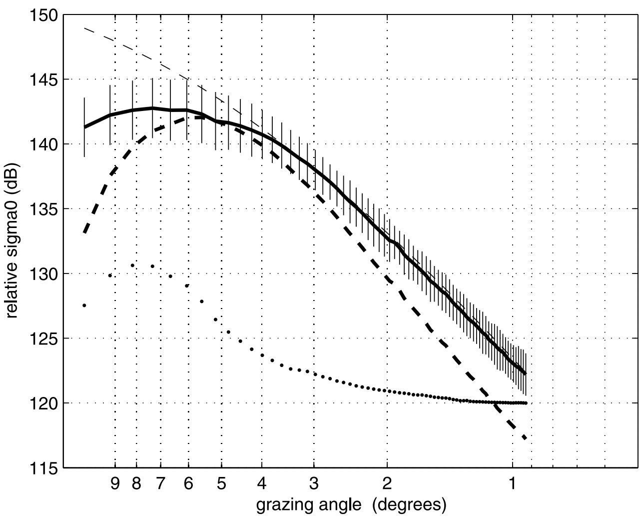

Figure 15. Variations of the mean relative backscattering coefficient in VV with grazing angle without (bold dashed line) and with (bold solid line) antenna pattern correction, of the scattering perturbation model expressed in equation (3) in relative value and omitting the Bragg wave spectral amplitude (thin dashed line) and of the mean noise level of Doppler spectra (bold dotted line). Vertical lines are error bars of length of two standard deviations.

is consistent with the description of the wave spectrum saturation range proposed by *Phillips* [1958] (considered also in the standard Pierson-Moskowitz spectrum, recently revisited by *Alves et al.* [2003]). The importance of non-linear energy transfers among waves, which increases with wave number, should explain the tendency toward an isotropic angular distribution of wave energy in the upwind angular sector. However, it should be mentioned that other wave [e.g., *Hwang*, 1997] and radar [e.g., *Donelan and Pierson*, 1987] measurements support a measurable dependency of radar backscatter on wind speed, which is the foundation of wind scatterometry.

5.2. Variation of the Relative Vertically Polarized Backscattering Coefficient With Grazing Angle

[41] According to the radar equation, σ^0_{VV} is proportional to $E_{VV}.r^3$ [*Skolnik*, 1980]. This quantity can thus be considered as an estimate of the relative backscattering coefficient, σ^0_{VVrel}. As the radial distance is a known function of grazing angle, variations of $E_{VV}.r^3$ with distance then reflect variations of σ^0_{VVrel} with α. Figure 15 shows these variations before and after antenna gain weighting factor correction (Figure 3). From slightly rough surface scattering theory, σ^0_{VVrel} is proportional to $f_{VV}(\alpha)$ given by [*Valenzuela*, 1978]:

$$f_{VV}(\alpha) = G(\alpha)\psi(\mathbf{\kappa_B}), \tag{3}$$

with

$$G(\alpha) = \sin^4\alpha \left| \frac{\varepsilon_r(1+\cos^2\alpha) - \cos^2\alpha}{\left(\varepsilon_r \sin\alpha + (\varepsilon_r - \cos^2\alpha)^{1/2}\right)^2} \right|^2$$

and $\psi(\boldsymbol{k_B})$ the two-dimensional spectrum of ocean waves evaluated at the Bragg wave number $\boldsymbol{k_B}$. Here ε_r is the complex dielectric constant of seawater (a value of 77–j66 was considered). G(α) represents quite well the observed variations of σ^0_{VVrel} for $\alpha < 3°$ (Figure 15). In that range of grazing angle values, σ^0_{VVrel} can be modeled by a power behavior in α^n with n = 3.15 (sd = 0.42) whereas from (3) n = 3.14. We verified that the theoretical value of n was negligibly modified by taking into account the slight damping of $\psi(\boldsymbol{k_B})$ as α decreases resulting, for a shape of ψ in k^{-4}, in a variation of f_{VV} in $\tan^4\alpha$ instead of $\sin^4\alpha$ in (3) [*Trizna*, 1996]. Furthermore, no significant variation of n with wind direction was detected, which reflects the observed insensitivity of the backscattered power to wind (section 5.1). The agreement between measured σ^0_{VVrel} values and the model described by (3) at low grazing angles was already reported by *Trizna* [1996] (n between 4 and 2.66).

[42] The departure of σ^0_{VVrel} from (3) for $\alpha > 3°$ can be interpreted, likely for the most important part, from saturation effects. We did not collect time series to confirm saturation of radar signals at short ranges. However, a signature of saturation effects can be found in the values of the noise level of the spectra, B. B is defined as the intrinsic noise floor level of each spectrum, B_f, divided by the ambient noise level, B_{env}. B_f was computed from the algorithm of *Hildebrand and Sekhon* [1974] and B_{env} by an histogram method applied to spectra at far ranges. σ^0_{VVrel} differ from $f_{VV}(\alpha)$ for grazing angles corresponding to a significant increase of B, which suggests a bias of back-scattered power values resulting from saturation. The influence of saturation in Doppler spectra in case of strong saturation was studied and modeled by *Forget et al.* [2003a]. A major effect of saturation resulted in an increase of Doppler spectral amplitudes on both sides of the central part of the spectrum, including the Bragg peaks, without significantly modifying the shape and position of the peaks. In the present experiment, saturation was not as strong, as it could be qualitatively observed on the scope. Then it can be reasonably expected that the results presented in sections 3–4 are little affected by saturation. An other reason for the departure of σ^0_{VVrel} from (3) might also come from the antenna pattern, which was not measured during the experiment and for which we have only the nominal characteristics.

5.3. Variation of the HH/VV Backscattering Polarization Ratio With Grazing Angle

[43] The energies used to compute this ratio, R, result from the summation over the whole spectral range of amplitudes that are greater than B_f. Only the radar cells that were not contaminated by possible effects of saturation (<3°) were considered. Given the characteristics of the radar, the precision on R values is expected to be quite good (less than few dB) (section 2.2).

[44] R measurements are shown versus α in Figure 16. The data are well organized according to the three main classes of wind-wave conditions which were already encountered in section 4: low winds, high winds/cross-wave conditions (beam directions 210° for wind event (E1) and 120° for (E2)) and high winds/up wave conditions (120° for (E1) and 210° for (E2)). In the first case, the range of

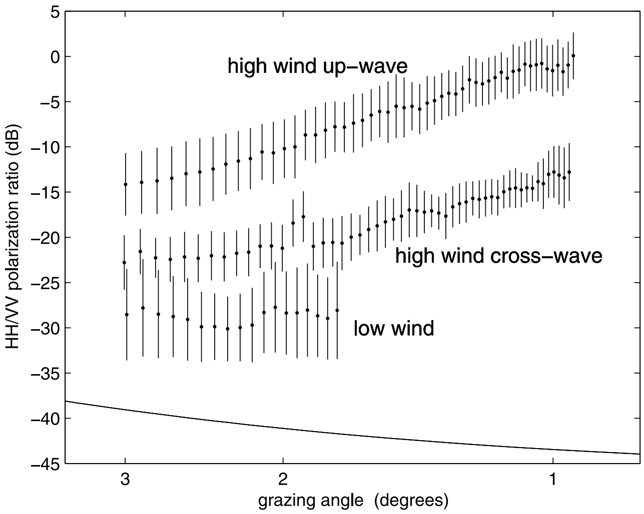

Figure 16. Variations of the HH/VV polarization ratio with grazing angle. Vertical lines are error bars. Lower curve is model (4).

α values is limited to 1.8°–3° because the signal-to-noise ratio of HH signals was too low for smaller angles (corresponding to larger distances from the radar).

[45] At low winds, the mean value of R was −28.8 dB with no significant variation with α. From first-order scattering theory, a model of R is given by [*Valenzuela*, 1978]:

$$R_{th}(\alpha) = \left| \frac{\left(\varepsilon_r \sin\alpha + (\varepsilon_r - \cos^2\alpha)^{1/2}\right)^2}{(\varepsilon_r(1+\cos^2\alpha) - \cos^2\alpha)\left(\sin\alpha + (\varepsilon_r - \cos^2\alpha)^{1/2}\right)^2} \right|^2. \tag{4}$$

R_{th} is plotted on Figure 16. A large difference, of the order of 10 dB, exists between R and R_{th} values. Such a difference was already reported in X band [*Lee et al.*, 1995] and S band [*Poulter et al.*, 1994] in similar conditions of "slow signals" and for α = 5°. According to the latter authors, a major reason for this difference is the strong hypothesis of a slightly rough surface underlying (4). Effects of long waves, which contribute to tilt the surface of the sea, can dramatically increase the R ratio at low grazing angles. This can be reproduced using the standard two-scale model [*Wright*, 1968] with possible improvements, e.g., by introducing curvature and shadowing effects [*Voronovich and Zavorotny*, 1998]. In our case, long waves in low-wind conditions would correspond to the swell phenomenon that was always observed at sea from the boat (Figure 1) and seen on measured wave spectra. Modeling exercises on present data are left for future works.

[46] For given grazing angle, values of the polarization ratio at high winds were greater than in the low-wind case. R increases from −22.2 dB (α = 3°) to −13.8 dB (α = 0.9°) in cross-wave conditions and from −13.9 dB to −1.1 dB in up wave conditions. Such high values of R, which can approach one, have been already observed [*Lee et al.*, 1995, 1996; *Smith et al.*, 1996]. By curve fitting the data points and considering the variation with α obtained for σ^0_{VVrel}, the relative backscattering coefficient in HH varies as $\alpha^{1.06}$ and $\alpha^{0.16}$ for cross-wave and up wave conditions, respectively. The exponents of α dramatically differ from the theoretical value of the exponent (=4) for the first-order relative backscattering coefficient $f_{HH}(\alpha)$ that can be obtained from (3) and (4).

[47] These results confirm that non-Bragg scattering effects play a major role in HH polarization and for high-wind–high-wave conditions, even when Doppler spectra do not exhibit fast scatterers (cross-wave radar look direction).

6. Summary and Perspectives

[48] The remote sensing experiment by coherent L band radar described in this paper offered a unique set of dual-polarized sea Doppler spectra at low grazing angles and for quite a large variety of wind and wave conditions.

[49] HH Doppler spectra at low wind and VV spectra from low to strong wind show a similar morphology, which is consistent with first- and higher-order electromagnetic wave surface–wave interaction processes of Bragg type.

[50] In VV polarization in general and in HH polarization at low wind, the shift of the Doppler spectral peak from Bragg wave velocity could be explained by surface current effects. Radar estimates of the current agreed with measurements performed at sea in low-wind conditions. At high wind, surface current values in VV are consistent with wind-induced drift currents. Coherent dual-polarized L band radar can then be useful for investigating dynamical aspects of the upper layer of the ocean. A similar conclusion was drawn by *Allan et al.* [1999] concerning high-resolution dual-polarized Doppler radars.

[51] In high-wind conditions, fast scatterers, i.e., those associated with Doppler velocities much greater than the Bragg wave velocity, were generally observed in HH Doppler spectra. The complex nearshore environment of the experiment was suitable to specify the influence of the wind and of the long waves of the wave spectrum on the occurrence of these fast scatterers. Wave modeling results demonstrated that wind and wave directions could be very different and that fast scatterers occurred in HH spectra in up/down wave (and not in cross wave) conditions, independently of the wind direction. The non-Bragg scattering mechanisms observed in HH polarization were also detected in VV Doppler spectra. These resulted in an increase of the spectral amplitudes in the velocity intervals were fast scatterers were present on the corresponding HH spectra.

[52] Vertically polarized backscattered energy was nearly insensitive to wind speed and direction. An explanation for that was given in terms of short-wave properties already reported in some wave experiments.

[53] The behavior of the backscattered energy with grazing angle for vertical polarization was found to agree quite well with the slightly rough surface scattering theory for the present range of low α values, except for the highest values, for which saturation effects of the radar signals were highly suspected.

[54] The HH/VV polarization ratio was found greater than predicted by the slightly rough surface scattering theory. At high winds, polarization ratio data could be classified according to long-wave conditions.

[55] Present observations of HH Doppler signatures and HH backscattered energy show that, as pointed out by many authors, a satisfactory theory remains to be developed to model horizontally polarized spectra at microwaves and especially at low grazing angles. Numerous processes that must be taken into account have already been mentioned in literature: scattering by bound tilted waves, by breaking waves or whitecaps, multiple scattering, shadowing effects etc.

[56] A dedicated experiment is planned in order to further investigate the L band coherent signature of backscattered radar signals from the sea surface. Specifically, we are planning to increase the spectral resolution, which was found insufficient here to separate the Bragg lines from the spectral continuum, or to detect spectral lines that can be expected from theory such as swell lines, harmonic lines, etc. Copolarization and cross polarization will also be measured during this future experiment.

[57] **Acknowledgments.** This work was funded by the department Sciences et Technologies de l'Information et de la Communication of Centre National de la Recherche Scientifique in the frame of Equipe Projet Multi-Laboratoires 38. The authors are grateful to colleagues of the laboratory (Y. Barbin and J. Gaggelli) and to Degréane Horizon Company (P. Currier and S. Caillet) who participated to the experiment.

References

Allan, N., C. L. Trump, D. B. Trizna, and D. J. McLaughlin (1999), Dual-polarized Doppler radar measurements of oceanic fronts, *IEEE Trans. Geosci. Remote Sens.*, *37*, 395–417.
Alves, J. H. G. M., M. Banner, and I. R. Young (2003), Revisiting the Pierson-Moskowitz asymptotic limits for fully developed wind waves, *J. Phys. Oceanogr.*, *33*, 1301–1323.
Banner, M. L., I. S. F. Jones, and J. C. Trinders (1989), Wavenumber spectra of short gravity waves, *J. Fluid Mech.*, *198*, 321–344.
Barrick, D. E. (1972), Remote sensing of sea state by radar, in *Remote Sensing of the Troposphere*, edited by V. E. Derr, chap. 12, pp. 12.1–12.46, U.S. Gov. Print. Off., Washington, D. C.
Barrick, D. E. (1998), Grazing behavior of scatter and propagation above any rough surface, *IEEE Trans. Antennas Propag.*, *46*, 73–83.
Barrick, D., M. W. Evans, and B. L. Weber (1977), Oceans surface currents mapped by radar, *Science*, *198*, 138–144.
Bénech, B., S. Derrien, B. Campistron, S. Jacoby-Koaly, F. Girard, P. Currier, J. Dessens, E. Dupont, and B. Carrissimo (2000), UHF radar performance at low (200W) and high (4KW) transmitted power in atmospheric boundary layer measurements, paper presented at 9th International Workshop on Technical and Scientific Aspects of MST Radars, Sci. Comm. on Sol.-Terr. Phys., Toulouse, France, 13–18 March.
Broche, P., P. Forget, J. C. De Maistre, J. L. Devenon, and M. Crochet (1987), VHF radar for ocean surface current and sea state remote sensing, *Radio Sci.*, *22*, 69–75.
Donelan, M. A., and W. J. Pierson (1987), Radar scattering and equilibrium ranges in wind-generated waves with application to scatterometry, *J. Geophys. Res.*, *92*, 4971–5029.
Duncan, J. R., W. C. Keller, and J. W. Wright (1974), Fetch and wind speed dependence of Doppler spectra, *Radio Sci.*, *9*, 809–819.
Ebuchi, N., H. Kawamura, and Y. Toba (1992), Statistical properties of microwave backscattering from laboratory wind-wave surfaces, *J. Oceanogr.*, *48*, 139–154.
Ebuchi, N., H. Kawamura, and Y. Toba (1993), Physical processes of microwave backscattering from laboratory wind wave surfaces, *J. Geophys. Res.*, *98*, 14,669–14,681.
Forget, P., P. Broche, J. C. De Maistre, and A. Fontanel (1981), Sea state frequency features observed by ground wave HF Doppler radar, *Radio Sci.*, *16*, 917–925.
Forget, P., J. L. Devenon, J. C. De Maistre, P. Broche, and M. Leveau (1990), VHF remote sensing for mapping river plume circulation, *Geophys. Res. Lett.*, *17*, 1097–1100.
Forget, P., Y. Barbin, P. Currier, and M. Saillard (2003a), Radar sea echo in UHF in coastal zone: Experimental observations and theory, paper presented at IGARSS 2003, Geosci. and Remote Sens. Soc., Toulouse, France, 21–25 July.
Forget, P., P. Broche, Y. Barbin, P. Currier, and M. Saillard (2003b), Observation of the coastal sea by L-band coherent radar, paper presented at SEE Workshop on Radar and Marine Environment, Soc. de Electr. et des Technol. de Inf. et de la Commun., Brest, France.
Guinard, N. W., J. T. Ransone, and J. C. Daley (1971), Variation of the NRCS of the sea with increasing roughness, *J. Geophys. Res.*, *76*, 1525–1538.
Hayslip, A. R., J. T. Johnson, and G. Baker (2003), Further numerical studies of backscattering from time-evolving nonlinear surfaces, *IEEE Trans. Geosci. Remote Sens.*, *41*, 2287–2293.
Hildebrand, P. H., and R. S. Sekhon (1974), Objective determination of the noise level in Doppler spectra, *J. Appl. Meteorol.*, *13*, 808–811.
Hwang, P. A. (1997), A study of the wavenumber spectra of short water waves in the ocean. part II: Spectral model and mean square slope, *J. Phys. Oceanogr.*, *14*, 1174–1186.
Johnson, J. T., J. V. Toporkov, and G. S. Brown (2001), Numerical study of backscattering from time-evolving sea surfaces: Comparison of hydrodynamic models, *IEEE Trans. Geosci. Remote Sens.*, *39*, 2411–2420.
Lamont-Smith, T. (2003), An empirical model of EM scattering from steepening wave profiles derived from numerical computations, *IEEE Trans. Geosci. Remote Sens.*, *41*, 1447–1454.
Lee, P. H. Y., J. D. Barter, K. L. Beach, C. L. Hindman, B. M. Lake, H. Rungaldier, J. C. Shelton, A. B. Williams, R. Yee, and H. C. Yuen (1995), X band microwave backscattering from ocean waves, *J. Geophys. Res.*, *100*, 2591–2611.
Lee, P. H. Y., J. D. Barter, E. Caponi, C. L. Hindman, B. M. Lake, and H. Rungaldier (1996), Wind-speed dependence of small-grazing-angle microwave backscatter from sea surfaces, *IEEE Trans. Antennas Propag.*, *44*, 333–340.
Lee, P. H. Y., J. D. Barter, K. L. Beach, B. M. Lake, H. Rungaldier, H. R. Thompson, and R. Yee (1998), Scattering from breaking gravity waves without wind, *IEEE Trans. Antennas Propag.*, *46*, 14–26.
Lee, P. H. Y., J. D. Barter, K. L. Beach, B. M. Lake, H. Rungaldier, H. R. Thompson, L. Wang, and R. Yee (1999), What are the mechanisms for non-Bragg scattering from water surfaces?, *Radio Sci.*, *34*, 123–138.
Lipa, B. J., and D. E. Barrick (1986), Extraction of sea state from HF radar sea echo: Mathematical theory and modeling, *Radio Sci.*, *21*, 81–100.
Liu, P. C., D. J. Schwab, and J. R. Bennett (1984), Comparison of a two-dimensional wave prediction model with synoptic measurements in Lake Michigan, *J. Phys. Oceanogr.*, *14*, 1514–1518.
Liu, P. C., D. J. Schwab, and R. E. Jensen (2002), Has wind-wave modeling reached its limit?, *Ocean Eng.*, *29*, 81–98.
Madsen, O. (1977), A realistic model of the wind-induced Ekman boundary layer, *J. Phys. Oceanogr.*, *7*, 248–255.
Phillips, O. M. (1958), The equilibrium range in the spectrum of wind-generated waves, *J. Fluid Mech.*, *4*, 426–434.
Plant, W. (1997), A model for microwave Doppler sea return at high incidence angles: Bragg scattering from bound, tilted waves, *J. Geophys. Res.*, *102*, 21,131–21,146.
Plant, W. J., and W. Keller (1990), Evidence of Bragg scattering in microwave Doppler spectra of sea return, *J. Geophys. Res.*, *95*, 16,299–16,310.
Plant, W. J., W. C. Keller, V. Hesany, T. Hara, E. Bock, and M. Donelan (1999), Bound waves and Bragg scattering in a wind-wave tank, *J. Geophys. Res.*, *104*, 3243–3263.
Poulter, E. M., M. J. Smith, and J. A. McGregor (1994), Microwave backscatter from the sea surface: Bragg scattering by short gravity waves, *J. Geophys. Res.*, *95*, 7929–7943.
Rozenberg, A. D., D. C. Quigley, and W. K. Melville (1996), Laboratory study of polarized microwave scattering by surface waves at grazing incidence; the influence of long waves, *IEEE Trans. Geosci. Remote Sens.*, *34*, 1331–1342.
Rozenberg, A. D., M. J. Ritter, W. K. Melville, C. C. Gottschall, and A. Smirnov (1999), Free and bound capillary waves as microwave scatterers: Laboratory studies, *IEEE Trans. Geosci. Remote Sens.*, *37*, 1052–1065.
Schwab, D. J., J. R. Bennett, P. C. Liu, and M. A. Donelan (1984), Application of a simple numerical wave prediction model to Lake Erie, *J. Geophys. Res.*, *89*, 3586–3592.
Skolnik, M. I. (1980), *Introduction to Radar Systems*, p. 472, McGraw-Hill, New York.
Sletten, M. A., and J. C. West (2003), Radar investigations of breaking water waves at low grazing angles with simultaneous high-speed optical imagery, *Radio Sci.*, *38*(6), 1110, doi:10.1029/2002RS002716.
Smith, M. J., E. M. Poulter, and J. A. McGregor (1996), Doppler radar measurements of wave groups and breaking waves, *J. Geophys. Res.*, *101*, 14,269–14,282.
Stewart, R. H., and J. W. Joy (1974), HF radio measurements of surface currents, *Deep Sea Res. Oceanogr. Abstr.*, *21*, 1039–1049.
Thompson, T. W., D. E. Weissman, and F. I. Gonzalez (1983), L band radar backscattter dependence upon surface wind stress: A summary of new SEASAT-1 and aircraft observations, *J. Geophys. Res.*, *88*, 1727–1735.

Toporkov, J. V., and G. S. Brown (2000), Numerical simulations of scattering from time-varying, randomly rough surfaces, *IEEE Trans. Geosci. Remote Sens.*, *38*, 1616–1625.

Toporkov, J. V., and G. S. Brown (2002), Numerical study of the extended Kirchhohh approach and the lowest order small slope approximation for scattering from ocean-like surfaces: Doppler analysis, *IEEE Trans. Antennas Propag.*, *50*, 417–425.

Trizna, D. B. (1996), Studies of dual polarized low grazing angle radar sea scatter in nearshore regions, *IEEE Trans. Geosci. Remote Sens.*, *34*, 747–757.

Valenzuela, G. (1974), The effect of capillarity and resonant interactions on the second-order Doppler spectrum of radar sea echo, *J. Geophys. Res.*, *79*, 5031–5037.

Valenzuela, G. (1978), Theories for the interaction of electromagnetic and oceanic waves—A review, *Boundary Layer Meteorol.*, *13*, 61–85.

Voronovich, A. G., and V. U. Zavorotny (1998), Curvature effects in the composite model for low-grazing-angle rough-surface scatter, *Waves Random Media*, *8*, 41–52.

Wright, J. W. (1968), A new model for sea clutter, *IEEE Trans. Antennas Propag.*, *AP-16*, 217–223.

Wright, J. W. (1978), Detection of ocean waves by microwave radar: The modulation of short gravity-capillary waves, *Boundary Layer Meteorol.*, *13*, 87–105.

P. Broche, P. Forget, and M. Saillard, Laboratoire de Sondages Electromagnétiques de l'Environnement Terrestre, CNRS, Université du Sud Toulon-Var, BP 132 La Garde, F-83957 France. (philippe.forget@lseet.univ-tln.fr)